APMA E4301 SPRING 2024 FINAL PROJECT
NUMERICAL SIMULATIONS OF THE ALLEN-CAHN EQUATION

KAIWEN ZHANG

1. Introduction and Setup

In this project, we consider the following IBVP, known as the Allen-Cahn equation or Ginzburg-Landau equation:

$$u_t = \Delta u + \frac{1}{\epsilon^2}(u - u^3), u : \Omega = [0,1]^2 \to \mathbb{R}, IC : u(0,x,y) = f(x,y), \tag{1}$$

$$BC : u(t,0,y) = u(t,1,y), u_x(t,0,y) = u_x(t,1,y), u(t,x,0) = u(t,x,1), u_y(t,x,0) = u_y(t,x,1). \tag{2}$$

i.e. with periodic boundary conditions.

The Allen-Cahn equation is motivated by the physical phenomenon of phase transitions. The Laplacian is a diffusive term, while the nonlinear term pushes the solution to take values of -1 and 1. To see this, observe that the ODE

$$u_t = u - u^3 = u(1+u)(1-u) \tag{3}$$

has an unstable fixed point at $u = 0$ and stable fixed points $u = -1$ and $u = 1$. Hence, the two stable fixed points can represent two "phases" of matter, e.g., liquid and solid. The Allen-Cahn equation for this reason has applications in superconductivity theory and image recognition.

From a variational perspective, the Allen-Cahn equation is a gradient flow.

Lemma 1. *Suppose u solves $u_t = \Delta u + \frac{1}{\epsilon^2}(u - u^3)$ with periodic boundary conditions. Then, u evolves according to the gradient flow of an energy E defined as:*

$$E[\psi] = \frac{1}{2}\int_\Omega |\nabla \psi|^2 + \frac{1}{4\epsilon^2}\int_\Omega (\psi^2 - 1)^2 \tag{4}$$

Proof: Compute the directional derivative of E in some direction v at point ψ:

$$\partial_v E[\psi] = \lim_{\eta \to 0} \frac{1}{\eta}\left(E[\psi + \eta v] - E[\psi]\right) \tag{5}$$

$$= \lim_{\eta \to 0} \frac{1}{\eta}\left(\frac{1}{2}\int_\Omega |\nabla(\psi + \eta v)|^2 - |\nabla \psi|^2 + \frac{1}{4\epsilon^2}\int_\Omega ((\psi + \eta v)^2 - 1)^2 - (\psi^2 - 1)^2\right) \tag{6}$$

$$= \lim_{\eta \to 0} \frac{1}{\eta}\left(\frac{1}{2}\int_\Omega 2\eta \nabla\psi \nabla v + \frac{1}{4\epsilon^2}\int_\Omega (2\psi^2 - 2 + 2\eta\psi v)(2\eta\psi v + \eta^2 v^2)\right) \tag{7}$$

$$= \lim_{\eta \to 0} \frac{1}{\eta}\left(\int_\Omega -\eta v \Delta\psi + \frac{1}{4\epsilon^2}\int_\Omega 2\eta(\psi^2 - 1 + \eta\psi v)(2\psi v + \eta v^2)\right) \tag{8}$$

$$= \lim_{\eta \to 0} \int_\Omega -v\Delta\psi + \frac{1}{2\epsilon^2}\int_\Omega (\psi^2 - 1 + \eta\psi v)(2\psi v + \eta v^2) \text{ integration by parts} \tag{9}$$

$$= \int_\Omega -v\Delta\psi + \frac{1}{2\epsilon^2}\int_\Omega (\psi^2 - 1)(2\psi v) = \int_\Omega (-\Delta\psi + \frac{1}{\epsilon^2}\psi(\psi^2 - 1))v \tag{10}$$

$$= \left\langle -\Delta\psi - \frac{1}{\epsilon^2}(\psi - \psi^3), v\right\rangle_{L^2(\Omega)} \tag{11}$$

Hence, formally $-\Delta\psi - \frac{1}{\epsilon^2}(\psi - \psi^3) = \nabla E[\psi]$ is the "gradient" of energy E.

Then if $u_t = \Delta u + \frac{1}{\epsilon^2}(u - u^3)$, $u_t = -\nabla E[u]$. On one hand:

$$\partial_{u_t} E[u] = \langle \nabla E[u], u_t \rangle_{L^2(\Omega)} = -\|\nabla E[u]\|^2 = \min_v \partial_v E[u] \tag{12}$$

On the other hand,

$$\partial_{u_t} E[u] = \lim_{\eta \to 0} \frac{1}{\eta} \left(E[u + \eta u_t] - E[u] \right) \tag{13}$$

$$= \lim_{\eta \to 0} \frac{1}{\eta} \left(E[u(t+\eta, x, y)] - E[u(t, x, y)] \right) = \frac{d}{dt} E[u(t, x, y)] \tag{14}$$

Hence

$$\frac{d}{dt} E[u(t, x, y)] = -\|\nabla E[u]\|^2 = \min_v \partial_v E[u] \tag{15}$$

and therefore u follows the gradient flow of E (in the steepest descent direction). This energy consideration will play a role in stability analysis of numerical schemes for the Allen-Cahn equation.

In this project, by default we distretize Ω into an uniform grid $\{x_k, y_l\}_{0 \leqslant k,l \leqslant N}$, with grid size $h_x = h_y = h = \frac{1}{N}$, where $x_k = kh, y_l = lh$. Note that $x_N = 1, y_N = 1$, so by periodicity we have $u(x_N, y_l) = u(x_0, y_l), u(x_k, y_N) = u(x_k, y_0)$.

2. Fourier Analysis on the Unit Square

The periodic boundary conditions in our problem (1) makes spectral methods appealing. Since eigenfunctions of the Laplacian operator are complex exponentials (or sines and cosines), it is helpful to review facts in continuous and discrete Fourier analysis on the domain $[0, 1]^2$. A rigorous introduction to the following statements can be found in [4].

Definition 2. *Let $u : \Omega = [0, 1]^2 \to \mathbb{R}$ be piecewise continuous and satisfying periodic boundary conditions, then the (m, n)th Fourier coefficient of u is:*

$$\tilde{u}(m, n) = \int_\Omega u(x, y) e^{-2\pi i(mx+ny)} dxdy \tag{16}$$

The Fourier series associated with u is

$$S(u) = \sum_{m,n \in \mathbb{Z}} \tilde{u}(m, n) e^{2\pi i(mx+ny)} \tag{17}$$

Lemma 3. *(Eigenbasis of $L^2(R^2/\Omega)$) The functions $\phi_{m,n} = e^{2\pi i(mx+ny)}$ form an orthonormal basis of $L^2(R^2/\Omega)$, the space of L^2 functions periodic on the domain Ω. Moreover, they are eigenfunctions of the Laplace operator with*

$$\Delta\phi_{m,n} = -4\pi^2(m^2 + n^2)\phi_{m,n} \tag{18}$$

The Fourier coefficient of u and that of Δu are related by a factor:

Lemma 4. *(Continuum Fourier Coefficient and Laplacian) Let u be as in definition 2. Then*

$$\tilde{\Delta u}(m, n) = -4\pi^2(m^2 + n^2)\tilde{u}(m, n) \tag{19}$$

And the operator from a function to its Fourier coefficients is norm-preserving, capture by the continuum Parseval's identity:

Lemma 5. *(Continuum Parseval's Identity)*

$$\int_\Omega f(x, y) g(x, y) dxdy = \sum_{m,n \in \mathbb{Z}} \tilde{f}(m, n) \tilde{g}(m, n) \tag{20}$$

in particular

$$\|f\|_{L^2}^2 = \sum_{m,n\in\mathbb{Z}} |\tilde{f}(m,n)|^2 \tag{21}$$

Analogous to the continuum case, we can define a discrete Fourier transform (DFT).

Definition 6. *Given Ω and grid points $\{x_k, y_l\}_{0\leqslant k,l\leqslant N}$, the discrete Fourier transform of a discretized function u is*

$$\hat{u}(m,n) = \sum_{k,l=0}^{N-1} u(x_k,y_l)e^{-2\pi i(mx_k+ny_l)} \tag{22}$$

for $m,n = 0,1,...,N-1$.

Lemma 7. *(Discrete Inverse Fourier Transform) Recovery the values of u is given by the inversion formula:*

$$u(x_k,y_l) = \frac{1}{N^2}\sum_{m,n=0}^{N-1} \hat{u}(m,n)e^{2\pi i(mx_k+ny_l)} \tag{23}$$

Note that in the definitions the indices go up to only $N-1$, because of periodicity.

Proof: compute

$$\sum_{m,n=0}^{N-1} \hat{u}(m,n)e^{2\pi i(mx_k+ny_l)} = \sum_{m,n=0}^{N-1}\sum_{p,q=0}^{N-1} u(x_p,y_q)e^{-2\pi i(mx_p+ny_q)}e^{2\pi i(mx_k+ny_l)} \tag{24}$$

$$= \sum_{p,q=0}^{N-1} u(x_p,y_q)\sum_{m,n=0}^{N-1} e^{2\pi i[m(x_k-x_p)+n(y_l-y_q)]} = \sum_{p,q=0}^{N-1} u(x_p,y_q)\sum_{m,n=0}^{N-1} e^{2\pi i\frac{m(k-p)+n(l-q)}{N}} \tag{25}$$

$$= \sum_{p,q=0}^{N-1} u(x_p,y_q)\sum_{m=0}^{N-1} e^{2\pi i\frac{m(k-p)}{N}}\sum_{n=0}^{N-1} e^{2\pi i\frac{m(l-q)}{N}} \tag{26}$$

If $k \neq p$, apply the summation formula for geometric sum:

$$\sum_{m=0}^{N-1} e^{2\pi i\frac{m(k-p)}{N}} = \frac{1-e^{2\pi i\frac{N(k-p)}{N}}}{1-e^{2\pi i\frac{(k-p)}{N}}} = 0 \tag{27}$$

Thus, the only case among all $p,q = 0,...,N-1$ that yields a nonzero term is $p = k, q = l$

$$\sum_{m,n=0}^{N-1} \hat{u}(m,n)e^{2\pi i(mx_k+ny_l)} = u(x_k,y_l)N^2 \tag{28}$$

The analogue of differential operators in discrete spaces are difference operators. Moreover, there is also a discrete analogue of Lemma 4.

Lemma 8. *(Discrete Fourier Transform and Difference Operator) For a discretized function u defined on the grid points of Ω, define the discrete second difference operator $D_{hx}^2 + D_{hy}^2$ as:*

$$(D_{hx}^2 + D_{hy}^2)u(x_k,y_l) = \frac{1}{h^2}(4u(x_k,y_l) - u(x_{k+1},y_l) - u(x_{k-1},y_l) - u(x_k,y_{l+1}) - u(x_k,y_{l-1})) \tag{29}$$

Then

$$\widehat{(D_{hx}^2 + D_{hy}^2)}u(m,n) = -\frac{4}{h^2}\left(\sin^2(\pi mh) + \sin^2(\pi nh)\right)\hat{u}(m,n) \tag{30}$$

Proof: note that, for example

$$\sum_{k,l=0}^{N-1} u(x_{k+1},y_l)e^{-2\pi i(mx_k+ny_l)} = \sum_{k,l=0}^{N-1} u(x_{k+1},y_l)e^{-2\pi i(mx_{k+1}+ny_l)}e^{2\pi imh} = e^{2\pi imh}\hat{u}(m,n) \tag{31}$$

because $x_k = kh = \frac{k}{N}$

Thus

$$\widehat{(D_{hx}^2 + D_{hy}^2)}u(m,n) = \frac{1}{h^2}\left(e^{2\pi imh} + e^{-2\pi imh} - 2 + e^{2\pi inh} + e^{-2\pi inh} - 2\right)\hat{u}(m,n) \tag{32}$$

$$= \frac{2}{h^2}\left(\cos(2\pi mh) - 1 + \cos(2\pi nh) - 1\right)\hat{u}(m,n) \tag{33}$$

$$= -\frac{4}{h^2}\left(\sin^2(\pi mh) + \sin^2(\pi nh)\right)\hat{u}(m,n) \tag{34}$$

Finally, to study the stability of spectral methods, we will use the discrete Parseval's identity:

Lemma 9. *(Discrete Parseval's Identity) Let u be a discretized function defined on the grid points, and $\hat{u}$ be its discrete Fourier transform. Then,*

$$\|u\|_2^2 = \frac{1}{N^2}\|\hat{u}\|_2^2 \tag{35}$$

where the norms are defined as:

$$\|u\|_2^2 = \sum_{k,l=0}^{N-1} h^2|u(x_k,y_l)|^2 \tag{36}$$

Proof is similar to that of lemma 7.

Remark: in the definition, the h^2 factor is used to imitate the area element, thus approximating the continuum 2-norm. We have purposefully left out some boundary points. If we were to include all of them, i.e., $k,l = 0,1,...,N$, the weights on the boundary points will change to $\frac{h^2}{4}$ for the four corners, and $\frac{h^2}{2}$ for the rest. The $\frac{1}{N^2}$ factor will not temper with stability estimates, because when transferring from Fourier domain to physical domain, we will multiply both sides with it.

3. Forward Euler in Time and Spectral in Space Discrete Scheme

3.1. **Derivation.** To derive a first fully discrete scheme, observe that the solution u to problem 1 must satisfy:

$$\langle\phi, u_t\rangle = \langle\phi, \Delta u\rangle + \frac{1}{\epsilon^2}\langle\phi, u - u^3\rangle \qquad \forall\phi \in H^1(\Omega) \tag{37}$$

Discretize in space using a Galerkin approximation, by taking $u = \sum_{m,n=0}^{N-1}\tilde{u}(m,n)e^{2\pi i(mx+ny)}$ and choosing $\phi = e^{2\pi i(mx+ny)}$ for $m,n = 0,1,...,N-1$. Note the inner product includes a complex conjugate. Then the scheme becomes finite dimensional in space and relates the Fourier coefficients.

$$\tilde{u_t}(m,n) = -4\pi^2(m^2+n^2)\tilde{u}(m,n) + \frac{1}{\epsilon^2}\widetilde{u - u^3}(m,n) \qquad \forall\phi \in H^1(\Omega) \tag{38}$$

We cannot compute the Fourier coefficients exactly via computers because it involves an integral, but we could approximate that integral using a left-endpoint quadrature, and the result is the discrete Fourier transform. Moreover, we discretize in time via forward Euler. The final scheme is:

- given discrete $\{u^j(x_k,y_l)\}_{k,l=0}^{N-1}$, compute $\hat{u}^j(m,n)$ and $\{\widehat{(u-u^3)}^j(m,n)\}_{m,n=0}^{N-1}$
- compute $\hat{u}^{j+1}(m,n)$ via

$$\hat{u}^{j+1}(m,n) = \hat{u}^j(m,n) - 4k\pi^2(m^2+n^2)\hat{u}^j(m,n) + \frac{k}{\epsilon^2}\widehat{(u-u^3)}^j(m,n) \tag{39}$$

- invert the DFT from $\hat{u}^{j+1}(m,n)$ to find $\{u^{j+1}(x_k,y_l)\}_{k,l=0}^{N-1}$

3.2. **Analysis.** The truncation error could be dealt with using properties of discrete Fourier transform, and stability estimates are also easier in Fourier domain.

3.2.1. *Consistency.* Let $u(t,x,y)$ be the true solution. We study the truncation error in Fourier space:

$$\tau^{j+1}(\hat{u}) = \frac{\hat{u}(t_{j+1},m,n)-\hat{u}(t_j,m,n)}{k} + 4\pi^2(m^2+n^2)\hat{u}(t_j,m,n) - \frac{1}{\epsilon^2}\widehat{(u-u^3)}(t_j,m,n) \tag{40}$$

Now

$$\frac{\hat{u}(t_{j+1},m,n)-\hat{u}(t_j,m,n)}{k} = \hat{u}_t(t_j,m,n) + O(k) \tag{41}$$

and by definition of DFT, $\hat{u}_t(t_j,m,n)$ is the DFT of $u_t(t,x,y)$.

On the other hand, by lemma 8,

$$\widehat{(D_{hx}^2+D_{hy}^2)}u(t_j,m,n) = -\frac{4}{h^2}\left(\sin^2(\frac{2\pi mh}{2})+\sin^2(\frac{2\pi nh}{2})\right)\hat{u}(t_j,m,n) \tag{42}$$

$$= -\frac{4}{h^2}\left[\pi^2h^2(m^2+n^2)+O(h^4)\right]\hat{u}(t_j,m,n) \tag{43}$$

$$= -4\pi^2(m^2+n^2)\hat{u}(t_j,m,n) + O(h^2) \tag{44}$$

Hence

$$4\pi^2(m^2+n^2)\hat{u}(t_j,m,n) = -\widehat{(D_{hx}^2+D_{hy}^2)}u(t_j,m,n) + O(h^2) \tag{45}$$

Substitute 41 and 45 into the definition of truncation error to obtain:

$$\tau^{j+1}(\hat{u}) = \hat{u}_t(t_j,m,n) + O(k) - \widehat{(D_{hx}^2+D_{hy}^2)}u(t_j,m,n) + O(h^2) - \frac{1}{\epsilon^2}\widehat{(u-u^3)}(t_j,m,n) \tag{46}$$

Study the expression on right hand side in physical domain:

$$\hat{u}_t(t_j,m,n) - \widehat{(D_{hx}^2+D_{hy}^2)}u(t_j,m,n) - \frac{1}{\epsilon^2}\widehat{(u-u^3)}(t_j,m,n) \tag{47}$$

$$= DFT[u_t - (D_{hx}^2+D_{hy}^2)u - \frac{1}{\epsilon^2}(u-u^3)](t_j,m,n) \tag{48}$$

Since

$$u_t - (D_{hx}^2+D_{hy}^2)u - \frac{1}{\epsilon^2}(u-u^3) = u_t - \Delta u - \frac{1}{\epsilon^2}(u-u^3) + O(h^2) \tag{49}$$

the truncation error in Fourier space goes to zero as $h \to 0$.

3.2.2. *Stability.* For the fully explicit-Euler scheme, the time step faces limitations in order for the scheme to be stable. For a heuristic derivation, recall the scheme 39. In vector notation, we can write using lexicographical ordering:

$$\hat{U}^{j+1} = (I - 4k\pi^2\hat{D}_h^2)\hat{U}^j + \frac{k}{\epsilon^2}\left(\widehat{U^j-(U^j)^3}\right) \tag{50}$$

where $\hat{D}_h^2$ is a diagonal matrix and entries on the diagonal correspond to the (m^2+n^2) term in the element-wise scheme.

Because of the discrete Parseval's identity, it suffices to study the conditions under which $\|\hat{u}^{j+1}\| \leqslant \|\hat{u}^j\|$. Note that the biggest diagonal entry in $\hat{D}_h^2$ is $2(N-1)^2$. Therefore, k needs to be on the order of $\frac{1}{N^2} = h^2$ for stability in 2-norm. Clearly k also needs to be on the order of ϵ^2 in order for the scheme to not blow up. So as $h \to 0$, the constraint on k is predominantly caused by h and becomes more and more strict.

4. Semi Implicit Euler in Time and Spectral in Space Scheme

In terms of stability, implicit schemes often offer better flexibility for time step than explicit ones. Starting from the fully explicit Euler scheme 39, the Laplacian term can be easily treated implicitly, but the nonlinear term is not trivially solvable so we leave it as it is. This results in a semi-implicit Euler in time scheme:

- given $\{u^j(x_k, y_l)\}_{k,l=0}^{N-1}$, compute discrete Fourier transform $\hat{u}^j(m,n)$ and $\{\widehat{(u-u^3)}^j(m,n)\}_{m,n=0}^{N-1}$
- compute $\hat{u}^{j+1}(m,n)$ via

$$\hat{u}^{j+1}(m,n) = \frac{1}{1+4k\pi^2(m^2+n^2)}\left(\hat{u}^j(m,n) + \frac{k}{\epsilon^2}\widehat{(u-u^3)}^j(m,n)\right) \tag{51}$$

- invert the DFT from $\hat{u}^{j+1}(m,n)$ to find $\{u^{j+1}(x_k, y_l)\}_{k,l=0}^{N-1}$

The method is widespread in literature. For instance, in [1], the authors demonstrate that the semi-implicit scheme mitigates limitations on time step size.

4.1. **Analysis.**

4.1.1. *Consistency.* In this section we present another perspective on consistency analysis, using Fourier expansion. Let $u(t,x,y)$ be the true solution. We study the truncation error in Fourier space:

$$\tau^{j+1}(m,n) = \frac{\hat{u}(t_{j+1},m,n) - \hat{u}(t_j,m,n)}{k} + 4\pi^2(m^2+n^2)\hat{u}(t_{j+1},m,n) - \frac{1}{\epsilon^2}\widehat{(u-u^3)}(t_j,m,n) \tag{52}$$

$$= \hat{u}_t(t_j,m,n) + 4\pi^2(m^2+n^2)\hat{u}(t_j,m,n) - \frac{1}{\epsilon^2}\widehat{(u-u^3)}(t_j,m,n) + O(k) \tag{53}$$

$$= \widehat{\Delta u}(t_j,m,n) + 4\pi^2(m^2+n^2)\hat{u}(t_j,m,n) + O(k), \text{ since } u_t = \Delta u + \frac{1}{\epsilon^2}(u-u^3) \tag{54}$$

Compute the discrete Fourier transform of $u(t,x,y)$ discretized on the grid:

Lemma 10. *The DFT of discretized $u(t_j,x,y)$ relates to its Fourier coefficients $\tilde{u}(t_j,p,q)$ by*

$$\hat{u}(t_j,m,n) = N^2 \sum_{a,b\in\mathbb{Z}} \tilde{u}(t_j, m+aN, n+bN) \tag{55}$$

The lemma is proved by computations: first recall that

$$u(t_j,x,y) = \sum_{p,q\in\mathbb{Z}} \tilde{u}(t_j,p,q)e^{2\pi i(px+qy)} \tag{56}$$

Then, compute DFT for the complex exponentials (denote temporarily as $\phi_{p,q}$):

$$\widehat{\phi_{p,q}}(m,n) = \sum_{k,l=0}^{N-1} \phi_{p,q}(x_k, y_l) e^{-2\pi i(mx_k+ny_l)} = \sum_{k,l=0}^{N-1} e^{2\pi i(px_k+qy_l)} e^{-2\pi i(mx_k+ny_l)} \tag{57}$$

$$= \sum_{k,l=0}^{N-1} e^{2\pi i \frac{(p-m)k+(q-n)l}{N}} \qquad \text{recall } x_k = \frac{k}{N}, y_l = \frac{l}{N} \tag{58}$$

$$= \left(\sum_{k=0}^{N-1} e^{2\pi i \frac{(p-m)k}{N}} \right) \left(\sum_{l=0}^{N-1} e^{2\pi i \frac{(q-l)k}{N}} \right) \tag{59}$$

If $p-m$ is not an integer multiple of N, the complex exponent in the first sum is nonzero. Then, apply the formula for summing a geometric sequence:

$$\sum_{k=0}^{N-1} e^{2\pi i \frac{(p-m)k}{N}} = \sum_{k=0}^{N-1} \left(e^{2\pi i \frac{p-m}{N}} \right)^k = \frac{1 - e^{2\pi i \frac{(p-m)N}{N}}}{e^{2\pi i \frac{p-m}{N}}} = \frac{1-1}{e^{2\pi i \frac{p-m}{N}}} = 0 \tag{60}$$

If $p = m + aN, a \in \mathbb{Z}$,

$$\sum_{k=0}^{N-1} e^{2\pi i \frac{(p-m)k}{N}} = N \tag{61}$$

The same applies to q and l. Therefore,

$$\widehat{\phi_{p,q}}(m,n) = N^2 \text{ if } p = m + aN, q = n + bN \text{ and 0 otherwise.} \tag{62}$$

Apply the conclusion to the Fourier expansion of u, to obtain the conclusion in the lemma:

$$\hat{u}(t_j, m, n)k = N^2 \sum_{a,b \in \mathbb{Z}} \tilde{u}(t_j, m + aN, n + bN) \tag{63}$$

Next, apply lemma 10 to u and Δu. Recall by lemma 4 that

$$\Delta u(t_j, x, y) = \sum_{p,q \in \mathbb{Z}} -4\pi^2(p^2 + q^2)\tilde{u}(t_j, p, q) e^{2\pi i(px+qy)} \tag{64}$$

Therefore

$$\widehat{\Delta u}(t_j, m, n) = N^2 \sum_{a,b \in \mathbb{Z}} -4\pi^2((m + aN)^2 + (n + bN)^2)\tilde{u}(t_j, m + aN, n + bN) \tag{65}$$

Apply equation 65 to the truncation error to yield:

$$\tau^{j+1}(m,n) = \widehat{\Delta u}(t_j, m, n) + 4\pi^2(m^2 + n^2)\hat{u}(t_j, m, n) + O(k) \tag{66}$$

$$= N^2 4\pi^2 \sum_{a,b \in \mathbb{Z}} (m^2 + n^2 - (m + aN)^2 - (n + bN)^2)\tilde{u}(t_j, m + aN, n + bN) + O(k) \tag{67}$$

$$= N^2 4\pi^2 \sum_{a,b \in \mathbb{Z}, a,b \neq 0} -((m + aN)^2 + (n + bN)^2)\tilde{u}(t_j, m + aN, n + bN) + O(k) \tag{68}$$

Finally, we use the fact that even for rough initial data, the true solution to Allen-Cahn equation is smooth for $t > 0$ (this is highly nontrivial to prove because of nonlinearity, especially for rough IC). Therefore, its Fourier coefficients decay faster than any polynomial power, i.e., $\forall r \in \mathbb{N}$, there exists $C_{r,j}$ such that a Fourier coefficient $\tilde{u}(t_j, p, q)$ of u are bounded by $\frac{C_{r,j}}{p^r + q^r}$. For finite time, we can maximize over j. Then the infinite sum in truncation error can be controlled by any polynomial.

Hence we reach the conclusion for consistency analysis:

Theorem 11. *The semi-implicit Euler in time and spectral in space scheme is consistent up to arbitrary order, i.e., the truncation error can be $O(h^r)$ for any power r with a varying constant.*

4.1.2. *Stability.* Naïvely speaking, in the semi-implicit scheme, k no longer needs to be on the order of h^2, but still needs to be on the order of ϵ^2. This gives more freedom in time step as the spatial grid gets refined past the scale of ϵ.

In [5] and [3], the authors treated the nonlinear term in the equation as the "derivative" of a primitive function, and applied a Taylor expansion to compute energy estimates. Here we imitate this technique to give an energy stability observation.

Suppose we are at time step j, going to $j+1$. In the algorithm, we obtain the discretized function values $u^j(x_k, y_l)$ by inverting the discrete Fourier transform $\hat{u}^j(m,n)$. But we can also directly use the DFT values as Fourier coefficients and define a continuum function at step j as

$$u^j(x,y) = \frac{1}{N^2}\sum_{m,n=0}^{N-1} \hat{u}^j(m,n)e^{2\pi i(mx+ny)} \tag{69}$$

u^j will have the same values on (x_k, y_l) as those obtained by inverting DFT. We can then study $E(u^{j+1})$ and $E(u^j)$ where E is the energy defined as in lemma 1. In the following computations, the L^2 inner product is the continuum definition:

$$\langle u, v\rangle_{L^2} = \int_\Omega uv \tag{70}$$

Compute:

$$E(u^{j+1}) - E(u^j) = \frac{1}{2}\left(\|\nabla u^{j+1}\|_{L^2}^2 - \|\nabla u^j\|_{L^2}^2\right) + \frac{1}{\epsilon^2}\int_\Omega F(u^{j+1}) - F(u^j) \tag{71}$$

where

$$F(u) = \frac{1}{4}(u^2-1)^2 \tag{72}$$

Apply the identity as described in [3]

$$\langle a-b, 2a\rangle = \|a\|^2 - \|b\|^2 + \|a-b\|^2 \tag{73}$$

to $\|\nabla u^{j+1}\|_{L^2}^2 - \|\nabla u^j\|_{L^2}^2$ to obtain

$$E(u^{j+1}) - E(u^j) = \left\langle \nabla u^{j+1} - \nabla u^j, \nabla u^{j+1}\right\rangle_{L^2} - \frac{1}{2}\|\nabla u^{j+1} - \nabla u^j\|_{L^2}^2 + \frac{1}{\epsilon^2}\int_\Omega F(u^{j+1}) - F(u^j) \tag{74}$$

Using periodic boundary conditions, apply integration by part to the first term:

$$\left\langle \nabla u^{j+1} - \nabla u^j, \nabla u^{j+1}\right\rangle_{L^2} = \left\langle u^{j+1} - u^j, -\Delta u^{j+1}\right\rangle_{L^2} \tag{75}$$

For the last term apply a Taylor expansion

$$F(u^{j+1}) - F(u^j) = (u^{j+1}-u^j)F'(u^j) + \frac{F''(\zeta)}{2}(u^{j+1}-u^j)^2 \tag{76}$$

for some ζ. Recall the definition of F to find that

$$F'(u^j) = -(u^j - (u^j)^3) \tag{77}$$

Therefore, formally:

$$\begin{aligned}\frac{1}{\epsilon^2}\int_\Omega F(u^{j+1}) - F(u^j) &= \int_\Omega (u^{j+1}-u^j)(-\frac{1}{\epsilon^2}(u^j-(u^j)^3)) + \frac{F''(\zeta)}{2\epsilon^2}(u^{j+1}-u^j)^2 \\ &\leqslant \left\langle u^{j+1}-u^j, -\frac{1}{\epsilon^2}(u^j-(u^j)^3)\right\rangle_{L^2} + \frac{\sup|F''(\zeta)|}{2\epsilon^2}\|u^{j+1}-u^j\|_{L^2}^2\end{aligned} \tag{78}$$

Apply equations 75 and 78 to equation 74, we obtain:

$$E(u^{j+1}) - E(u^j) \leqslant \left\langle u^{j+1} - u^j, -\Delta u^{j+1} \right\rangle_{L^2} - \frac{1}{2}\|\nabla u^{j+1} - \nabla u^j\|_{L^2}^2 + \left\langle u^{j+1} - u^j, -\frac{1}{\epsilon^2}(u^j - (u^j)^3) \right\rangle_{L^2} + \frac{|\sup F''(\zeta)|}{2\epsilon^2}\|u^{j+1} - u^j\|_{L^2}^2 \tag{79}$$

Next we convert the L^2 inner products to inner product of Fourier coefficients using the continuum Parseval's identity (lemma 5). Because of the definition of u^j, its Fourier coefficients are simply $\frac{1}{N^2}\hat{u}^j$. The Fourier coefficient for $\Delta u(m,n)$ is a factor away from those of u.

A trouble is that the $u^j - (u^j)^3$ has Fourier modes with frequencies higher than $N-1$. In this case, the DFT of $u^j - (u^j)^3$ is no longer equal to the Fourier coefficients, but can be seen as a numerical quadrature approximation of the Fourier coefficients of $u^j - (u^j)^3$ with distance between sample points $\Delta x = h$. Then the Fourier coefficient of $u^j - (u^j)^3$ are at most $O(h^3)$ higher than the DFT, and the constant is no larger than the supremum of magnitude of derivative of $u^j - (u^j)^3$. Note also that although $u^j - (u^j)^3$ has Fourier coefficients beyond frequency $N-1$, but $u^{j+1} - u^j$ does not have such coefficients, the inner product for coefficients beyond frequency $N-1$ is zero. Hence:

$$E(u^{j+1}) - E(u^j) \leqslant \frac{1}{N^2}\sum_{m,n=0}^{N-1} \widehat{(u^{j+1} - u^j)} \left\{ 4(m^2+n^2)\hat{u}^{j+1}(m,n) - \frac{1}{\epsilon^2}\widehat{(u^j - (u^j)^3)} \right\} - \frac{1}{2}\|\nabla u^{j+1} - \nabla u^j\|_{L^2}^2 + \frac{|\sup F''(\zeta)|}{2\epsilon^2}\|u^{j+1} - u^j\|_{L^2}^2 + \frac{|\sup F''(\zeta)|}{\epsilon^2}h^3 \tag{80}$$

Now notice that due to the scheme,

$$4(m^2+n^2)\hat{u}^{j+1}(m,n) - \frac{1}{\epsilon^2}\widehat{(u^j - (u^j)^3)} = -\frac{\hat{u}^{j+1} - \hat{u}^j}{k} \tag{81}$$

So finally,

(82)

$$E(u^{j+1}) - E(u^j) \leqslant -\frac{1}{N^2}\left\{ \frac{1}{2}\|\nabla u^{j+1} - \nabla u^j\|_{L^2}^2 + \left[\frac{1}{k} - \frac{|\sup F''(\zeta)|}{2\epsilon^2}\right]\|u^{j+1} - u^j\|_{L^2}^2 - \frac{|\sup F''(\zeta)|}{\epsilon^2}h^3 \right\}$$

So, if $F''(u)$ were bounded, then for sufficiently small h,

$$k < \frac{2\epsilon^2}{\sup|F''(\zeta)|} = \frac{2\epsilon^2}{\sup|f'(\zeta)|} \tag{83}$$

where $f(u) = u^3 - u$ is a practical condition for energy stability. Note the condition gets more strict for smaller ϵ, as expected. Note also that in this case, if we have $h = O(\epsilon)$ then the last remainder term is $O(h)$ small, so not entirely hopeless. The condition $h = O(\epsilon)$ is not an unreasonable request, because ϵ is the length scale of the interface between two phases in the solution of the PDE ([5]).

Sadly, however, theoretically for our choice of $f(u) = u^3 - u$, $f'(u)$ is unbounded. For a particular initial value problem, if one knows by experience an approximate bound for the values of u at all times(say interval I), then one could use $\sup F''(\zeta)$ for $\zeta \in I$ to get a ballpark sense of how small k needs to be. This is not a rigorous proof though. Authors in [3] did mention, nevertheless, a way to modify the potential to achieve a boundedness property here. We finish this section with the following conclusion:

Theorem 12. *If $u - u^3$ were replaced by some other $f(u)$ with bounded derivative, then the numerical solution obtained by the semi-implicit spectral scheme obeys the energy estimate 82.*

4.2. **Numerical Experiments.** This section shows results of numerical experiments conducted using semi-implicit spectral methods. In the experiment we set numerous parameters: ϵ is the corresponding ϵ in the equation, T_f is terminal time, T_N is number of time steps, and N is grid discretization parameter where $h = 1/N$ is the grid size.

4.2.1. *Circular Initial Data.* For experiments 1 and 2, the initial condition is set to be 1 in a circle around $(\frac{1}{2}, \frac{1}{2})$, and -1 elsewhere. The specific parameters are given in table 1 (r^2 is the square of the circle in initial data):

Parameter	r^2	ϵ	T_f	T_N	N
Experiment 1	0.2	0.15	0.03	50	200
Experiment 2	0.12	0.12	0.03	20	50

Table 1. Parameters for Numerical Experiments with Circular Initial Data

The numerical results are shown in figure 1 and figure 2.

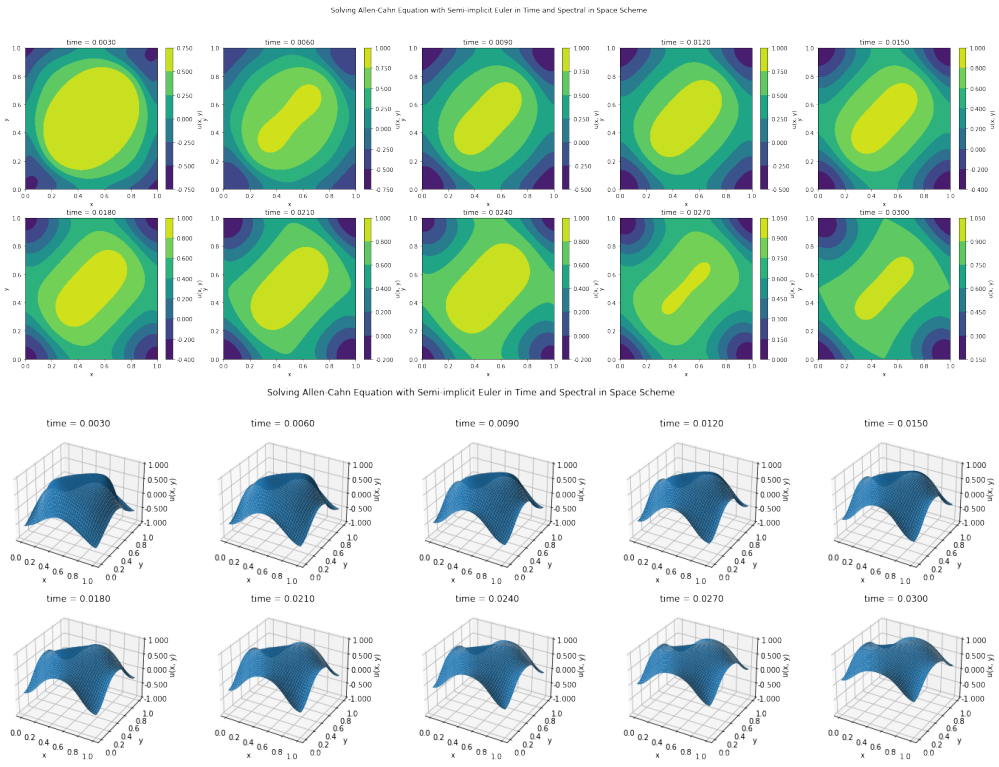

Figure 1. Numerical Results, Experiment 1

Both experiments show that the solution minimizes the phase separation, similar to the curve-shortening motion. Interestingly, in experiment 1 the solution converges to a steady state with constant 1, while in experiment 2 the solution converges to a constant state zero. This is not completely surprising. For instance, if there were ice and water in periodic squares, if initially there were a lot of ice, the steady state of the system would be completely frozen, but if initially there were lots of water, the steady state would be completely melt.

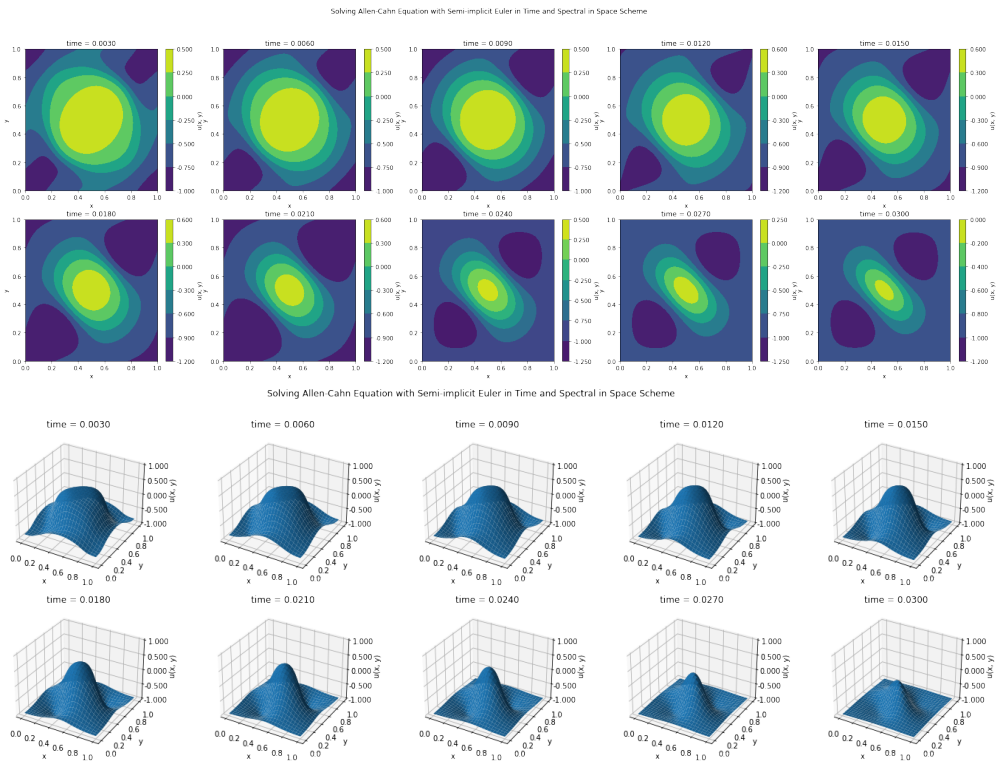

Figure 2. Numerical Results, Experiment 2

4.2.2. *Random Initial Data.* For experiments 3 and 4, the initial data is random. For experiment 3, the initial value on each grid point is chosen from an uniform distribution on interval $[-1, 1]$. For experiment 4, the initial value on each grid point is chosen from the discrete set $\{-1, 1\}$ with equal probability for each choice. The other parameters are shown in table 2:

Parameter	ϵ	T_f	T_N	N
Experiment 3	0.15	0.01	50	200
Experiment 4	0.1	0.01	50	200

Table 2. Parameters for Numerical Experiments with Random Initial Data

Initial conditions are shown in figure 3, and numerical results are shown in figures 4 and 5.

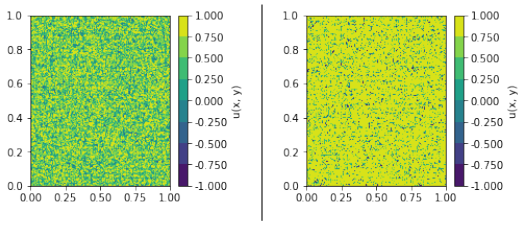

Figure 3. Random Initial Conditions for Experiments 3 and 4

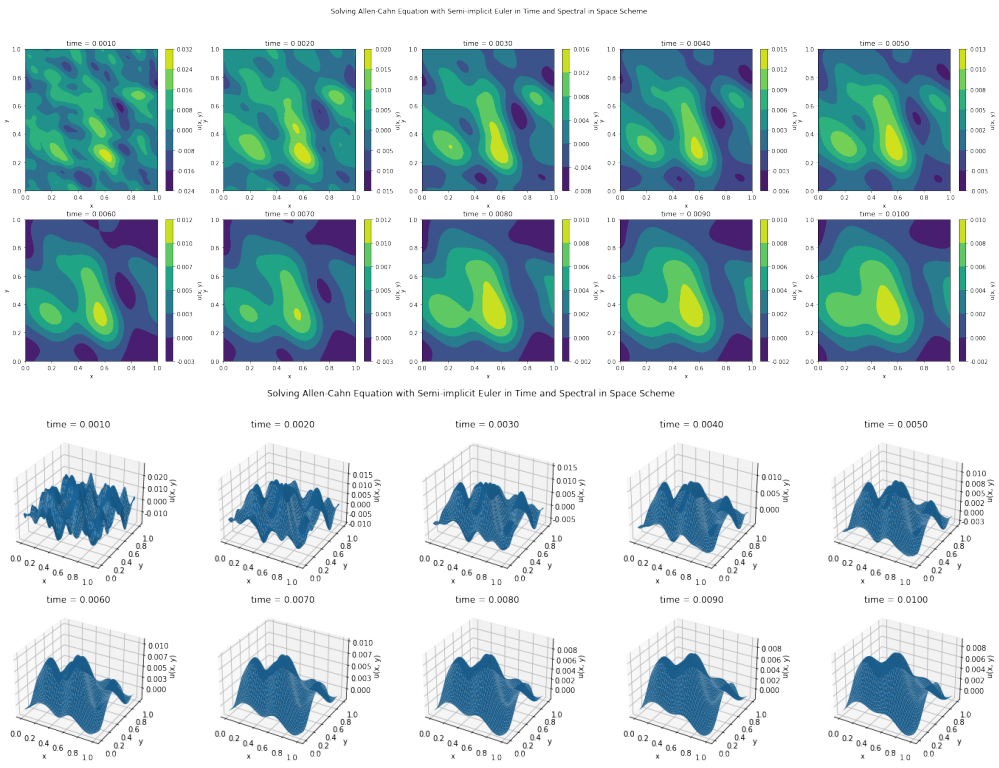

Figure 4. Numerical Results, Experiment 3

5. Fully Implicit Spectral Method via Optimization Formulation

5.1. **Derivation.** Inspired by lemma 1, one approach of forming a numerical scheme is the reproduce the gradient descent of energy discretely. This can be achieved by a semi-discretization in time that is fully implicit:

Lemma 13. *In semi-discrete scheme*

$$\frac{1}{k}(u^{j+1}-u^j) = \Delta u^{j+1} + \frac{1}{\epsilon^2}(u^{j+1}-(u^{j+1})^3) \tag{84}$$

given u^j, u^{j+1} solves a minimization problem involving a proximal operator, given by the following:

$$u^{j+1} = \arg\min_{\psi} \mathcal{F}^j[\psi] := \arg\min_{\psi}\left(E[\psi] + \frac{1}{2k}\|\psi - u^j\|_2^2\right) \tag{85}$$

Where E is the nonlinear energy defined in lemma 1. Moreover, in this scheme, the energy E is automatically decreasing from u^j to u^{j+1}.

Proof: At the minimizer of the semi-discretized energy, the directional derivative is zero for any direction v. Compute:

$$\partial_v \mathcal{F}^j[\psi] = \partial_v E[\psi] + \frac{1}{2k}\left\{\lim_{\eta\to 0}\frac{1}{\eta}\left(\|\psi+\eta v - u^j\|_2^2 - \|\psi - u^j\|_2^2\right)\right\} \tag{86}$$

$$= \int_\Omega (-\Delta\psi + \frac{1}{\epsilon^2}\psi(\psi^2-1))v + \frac{1}{2k}\int_\Omega 2(\psi-u^j)v \tag{87}$$

Thus, setting $\partial_v\mathcal{F}[\psi] = 0, \forall v$ yields

$$\frac{1}{k}(\psi - u^j) = \Delta\psi + \frac{1}{\epsilon^2}(\psi - \psi^3) \tag{88}$$

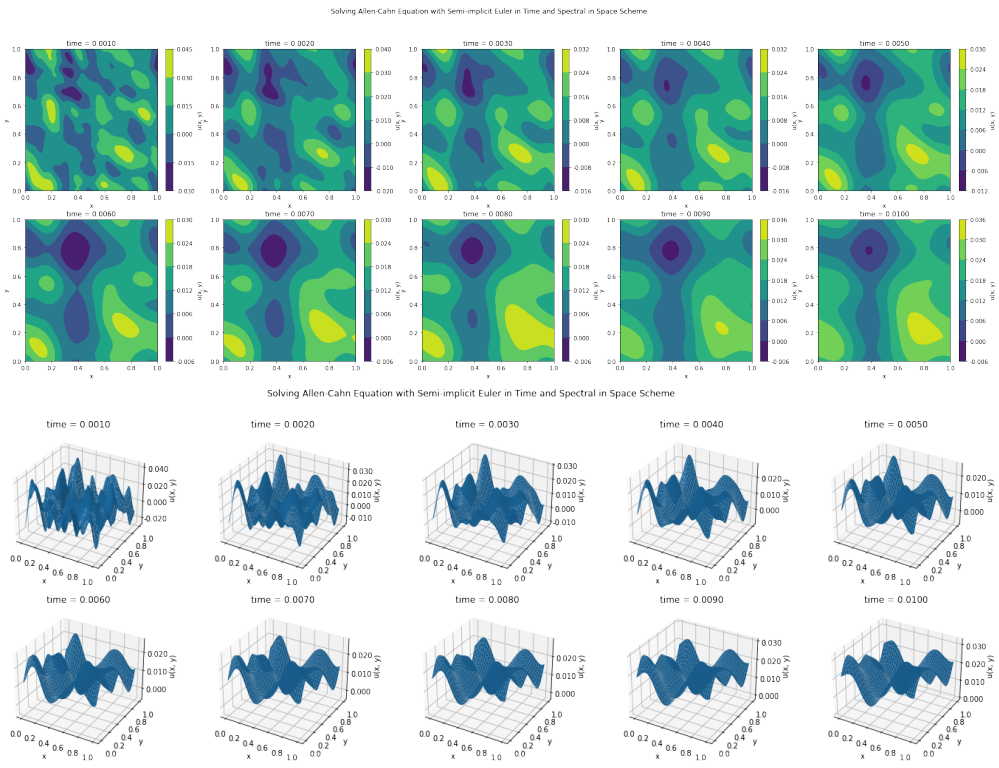

Figure 5. Numerical Results, Experiment 4

which is the desired semi-discrete scheme.

To see the decrease in energy, note that since u^{j+1} minimizes $\mathcal{F}^j$,

$$\mathcal{F}^j[u^{j+1}] \leqslant \mathcal{F}^j[u^j] \tag{89}$$

$$E[u^{j+1}] + \frac{1}{2k}\|u^{j+1} - u^j\|_2^2 \leqslant E[u^j] + 0 \tag{90}$$

$$E[u^{j+1}] \leqslant E[u^j] \tag{91}$$

If we were able use the fully implicit scheme, we would automatically achieve energy stability. However, this is an infinite dimensional optimization problem. To make it solvable numerically, we can solve it on the span of finitely many Fourier modes. The algorithm hence is given u^j, find u^{j+1} such that

$$u^{j+1} = \arg\min_{\psi \in V_N} \left(E[\psi] + \frac{1}{2k}\|\psi - u^j\|_2^2 \right) \tag{92}$$

where $V_N = span\{\sin(2\pi kx), \cos(2\pi kx), \sin(2\pi ky), \cos(2\pi ky)\}_{0 \leqslant k \leqslant N}$

The transition from semi-discrete to fully discrete scheme is not completely independent of grid points, because the distance $\|\psi - u^j\|_2^2$ has to be evaluated numerically as:

$$\|\psi - u^j\|_2^2 \approx \sum_{k,l=0}^{N-1} h^2(\psi(x_k, y_l) - u^j(x_k, y_l))^2 \tag{93}$$

The nonlinear energy term also needs to be evaluated numerically. The gradient term can be computed analytically because of orthogonality properties of cosines and sines. Specifically, the integral $\int_\Omega |\nabla\psi|^2$ is $2\pi^2k^2$ for a kth basis function.

If

$$\psi(x,y) = \sum_{k=0}^{N} A_k \sin(2\pi kx) + B_k \cos(2\pi kx) + C_k \sin(2\pi ky) + D_k \cos(2\pi ky) \tag{94}$$

Then

$$\begin{aligned}
&\frac{1}{2}\int_\Omega |\nabla\psi|^2 \\
&= \frac{1}{2}\sum_{k=0}^{N} A_k^2 \int_\Omega |\nabla \sin(2\pi kx)|^2 + B_k^2 \int_\Omega |\nabla \cos(2\pi kx)|^2 \\
&+ C_k^2 \int_\Omega |\nabla \sin(2\pi ky)|^2 + D_k^2 \int_\Omega |\nabla \cos(2\pi ky)|^2 \\
&= \frac{1}{2}\sum_{k=0}^{N} 2\pi^2k^2(A_k^2 + B_k^2 + C_k^2 + D_k^2) = \sum_{k=0}^{N} \pi^2k^2(A_k^2 + B_k^2 + C_k^2 + D_k^2)
\end{aligned}$$

5.2. **Numerical Experiment.** In experiment 5 and 6, we apply the fully implicit algorithm described above use circular initial data to contrast the result with experiments 1 and 2. The specific parameters are shown in table 3. N_{coef} is the highest frequency of Fourier mode used. There would be $N_{coef} + 1$ Fourier modes used in the optimization.

Parameter	r^2	ϵ	T_f	T_N	N	N_{coef}
Experiment 5	0.2	0.12	0.01	20	50	6
Experiment 6	0.12	0.12	0.03	20	50	9

Table 3. Parameters for Experiments with Circular IC, Implicit Optimization Scheme

The numerical results are shown in figures 6 and 7.

The evolution in experiment 5 is very slow, and the numerical results do not get as close to the constant steady state at the same time marks, compared to experiment 1. The slow evolution is not surprising, because in the energy defined in equation 92, a small time step puts a large weight on the proximal term, meaning the solution at next time step must stay close to the current step. The solutions look very regular, because of the low number of Fourier modes used. The reason for using a low number of Fourier modes is that the running time for the fully implicit optimization algorithm is extremely long.

Experiment 6 uses the same initial data, ϵ, grid size, and time step size as experiment 2, but the simulation is perhaps not as good, because in experiment 6 the numerical solution struggles to force values in the areas near the domain boundary down to -1. This should be again due to the small number of Fourier modes used. The reason for using a low number of Fourier modes is that the running time for the fully implicit optimization algorithm is extremely long. The code for experiment 6 ran for around 6.5 to 7 hours.

6. Concluding Remarks and Acknowledgement

In addition to the methods mentioned above, there are also time-splitting methods. In time-splitting schemes, for each step, one solves the diffusion PDE and the nonlinear ODE sequentially. The solution for the diffusion PDE is used as the initial condition when solving the remaining

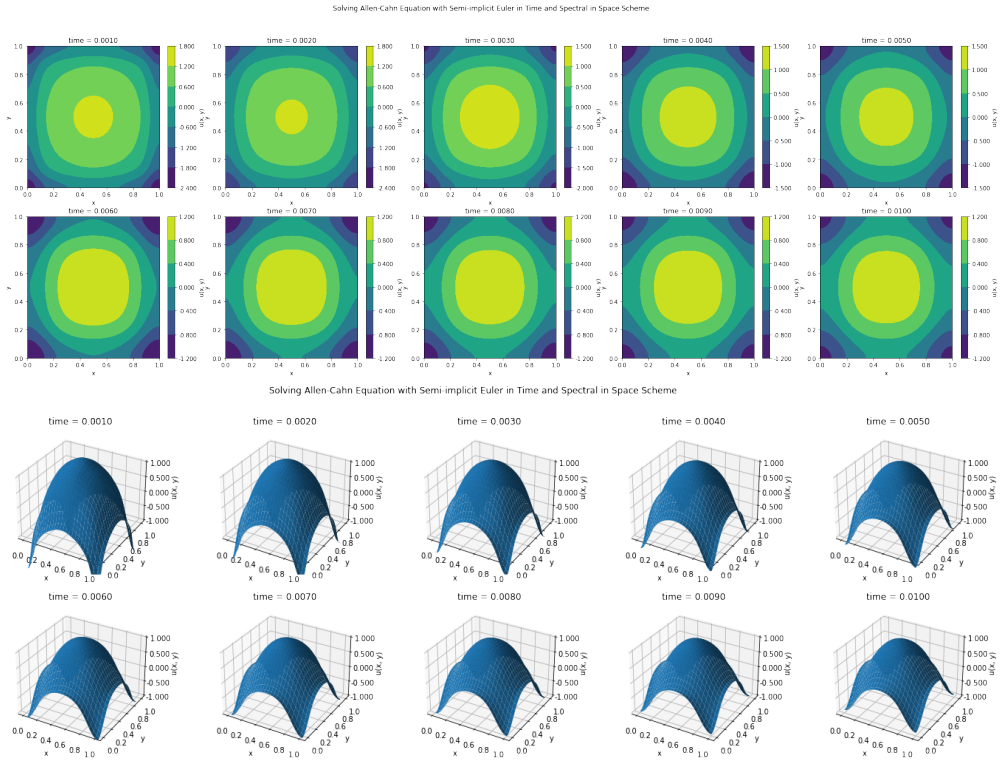

Figure 6. Numerical Results, Experiment 5

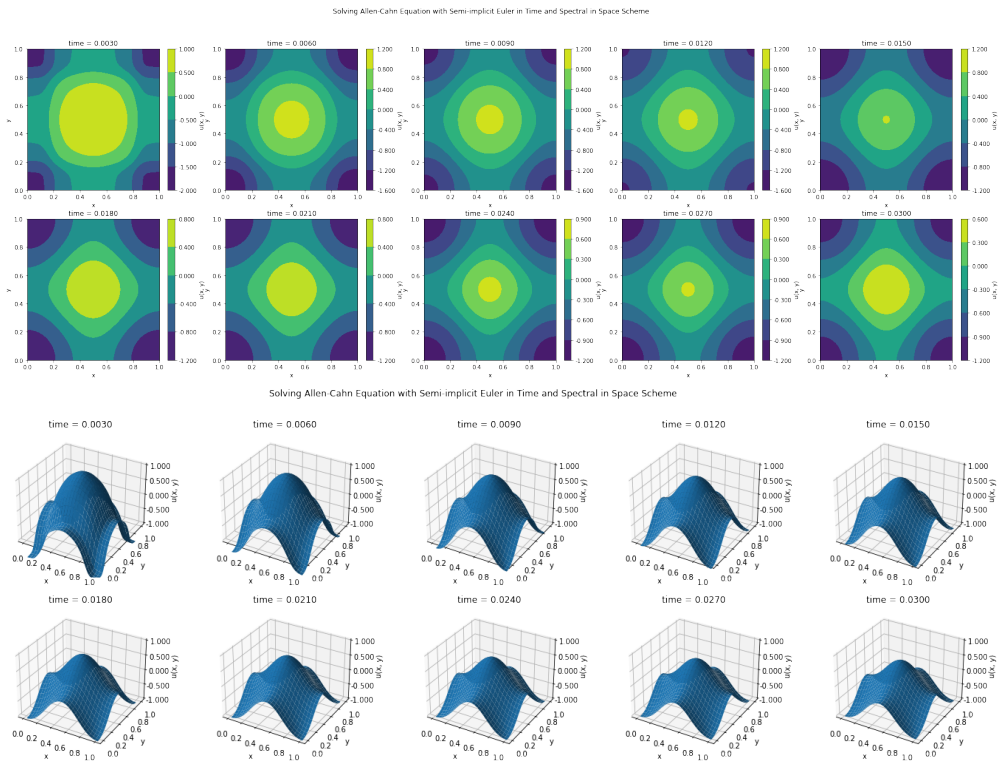

Figure 7. Numerical Results, Experiment 6

nonlinear ODE. In [2], the authors developed a time-splitting method in which both the diffusion and the nonlinear ODE are solved analytically. In this case, the error only comes from time-splitting.

Moreover, in the regime where ϵ is small, one can apply threshold dynamics developed by S. Esedoglu and collaborators. The idea is that instead of solving the nonlinear ODE in the second sub-step, one truncates the solution to diffusion by, for instance, assigning to negative initial values a new value of -1, and to all positive initial values a new value of +1. This algorithm is an approximation to the Allen-Cahn equation in a sense that the solution it produces is never smooth, but if one sees Allen-Cahn as a smoothed approximation to motions of sharp interfaces, then threshold dynamics is beneficial because it restores the sharpness at the interface.

This concludes the discussion of numerical simulations of the Allen-Cahn equation. The equation itself poses an interesting model for phase transitions, and the nonlinear term, while responsible for the phase-transition behavior, poses challenges for regularity and stability analysis.

I am extremely grateful to the peers who supported me during the Numerical PDEs course. In particular I thank Joonsoo Lee for helpful discussions on the stability estimates and directing me to previous literature. I wish to express my most sincere gratitude to Professor Qiang Du, whose guidance and help along the way has revealed to me the technical subtleties as well as the fun in numerical analysis.

References

[1] L. Q. Chen and J. Shen. "Applications of semi-implicit Fourier-spectral method to phase field equations". *Computer Physics Communications* 108.2-3 (1998), pp. 147–158.

[2] H. G. Lee and J.-Y. Lee. "A semi-analytical Fourier spectral method for the Allen–Cahn equation". *Computers & Mathematics with Applications* 68.3 (2014), pp. 174–184.

[3] J. Shen and X. Yang. "Numerical approximations of allen-cahn and cahn-hilliard equations". *Discrete Contin. Dyn. Syst* 28.4 (2010), pp. 1669–1691.

[4] E. Stein and R. Shakarchi. *Fourier Analysis: An Introduction*. Princeton University Press, 2003. ISBN: 9780691113845.

[5] J. Zhang and Q. Du. "Numerical studies of discrete approximations to the Allen–Cahn equation in the sharp interface limit". *SIAM Journal on Scientific Computing* 31.4 (2009), pp. 3042–3063.